Acoustic Meta-Equalizer

Yifan Zhu, Shi-Wang Fan, Liyun Cao, Krupali Donda, B. Assouar

Acoustic meta-equalizer

Yifan Zhu*, Shi-Wang Fan, Liyun Cao, Krupali Donda, and Badreddine Assouar*

Institut Jean Lamour, CNRS, Université de Lorraine, Nancy, 54000, France.

Abstract

Acoustic equalization is the process of adjusting the frequency response of a broadband sound signal, which is widely used in communication system and audio acoustics. Here, we introduce the unique concept of acoustic meta-equalizer, *viz.*, a passive acoustic metamaterial-based filter that has tunable frequency response within ultra-broadband (200Hz – 20000Hz), and capable to generate a frequency equalization on the input sound signal. By exploiting two kinds of acoustic resonant elements, *viz.*, Helmholtz and Fabry–Perot resonators, we realize and demonstrate ultra-broadband and tunable filters, within an integrated meta-structure. In analogy with the conventional equalizer concept in signal processing, we numerically, analytically, and experimentally demonstrate functional filters, signal reproductions, and sound effect controls by the conceived acoustic meta-equalizer.

Keywords: Acoustics, Metamaterials, Equalizer, Tunable filter, Ultra-broadband feature.

***Corresponding authors:**

yifan.zhu@univ-lorraine.fr

badreddine.assouar@univ-lorraine.fr

I. INTRODUCTION

Equalization is an important concept in signal processing, that is, adjusting the frequency response of a broadband signal. It has been and still widely used in telecommunications [1-3], and various acoustic applications including audio device [3-5], room acoustics [6-10] and underwater communications [11-12]. The resulting filter device is known as equalizer (EQ). The acoustic equalizer device can adjust the loudness curve of a broadband sound signal to improve the quality of audio sound, because the tone color of sound is influenced by different frequency ingredients [4-5]. In room acoustics [6-8], different complex acoustic environments will influence the uniformity of the frequency response, so that acoustic equalization can be used to reproduce the sound signals [6-8], or to realize active noise control [9-10]. In hydroacoustics, similarly, the complex environment makes the acoustic equalization process necessary in underwater acoustic communications [11-12].

On the other hand, during the last decade, acoustic metamaterials have been actively studied [13-14], providing different design strategy for various acoustic devices. For example, acoustic metamaterials have been proposed to actively control specific interesting acoustic phenomena such as cocktail effect [15], acoustic reverberation [16], and acoustic hologram [17]. Acoustic metamaterials are also exploited for underwater communications [18-19]. For the designs of sound absorber, acoustic metamaterials can bring a real added value to the absorption performance with large bandwidth and reduced sample thickness [20]. To further decrease the thickness of acoustic resonant units, the concept of acoustic metasurfaces was proposed [21] to design unconventional ultra-thin acoustic devices. For instance, a metasurface-based Schroeder diffuser design [22] is only 1/10 thickness of the conventional ones [23]. For sound absorber, deep-subwavelength metasurface-based absorber was evidenced [24], which is much thinner

than the absorber from classical materials, showing the great flexibilities and potentials of acoustic metamaterials and metasurfaces.

In this research, we extend the general concept of acoustic metamaterials to equalizer, by proposing the unique concept of acoustic meta-equalizer (AMEQ), *viz.*, a tunable and ultra-broadband passive acoustic metamaterial filter. Previous designs of acoustic filters [25-28] have shown limited bandwidth (narrow band) or limited amplitude values (only 0 and 1). Therefore, an ultra-broadband and tunable acoustic filter is highly desired for practical acoustic applications. In our proposed concept, the designed AMEQ can realize different specific amplitude controls with different values (-2dB to -10dB, with a step of -2dB) within ultra-broadband (200Hz-20000Hz). This design goal is realized by using two kinds of acoustic resonant elements, *viz.*, Helmholtz resonators (HRs) [29, 30] and Fabry–Perot resonators (FPRs), that is, an array of narrow tubes with different depths [20, 31]. We realize both low-frequency and high-frequency equalizations with these two acoustic elements, respectively, in an integrated acoustic meta-structure. Although these acoustic resonant elements have been demonstrated for sound absorption [20, 31, 32] before, realizing ultra-broadband filter is challenging due to the very large span of the targeted frequencies (7 octaves). This makes the size of whole structure sub-wavelength for low frequencies, but larger than wavelength for high frequencies. Therefore, the low frequency filters are owing to the coupled resonance of the whole structure, while the high frequency filters are determined by both the resonance of FPRs and geometry acoustics effect. This complex case requires deliberate design (including the geometric feature of the channel, the size and position of each resonator). It is distinct from conventional acoustic absorber designs, which will be demonstrated numerically, analytically, and experimentally in the following sections of this article.

We illustrate in Fig. 1 the classical EQ concept in different domains of applications. Figure 1(a) shows an audio EQ device, which is widely used in sound effects manipulations. Figure 1(b) exhibits the EQ software which can adapt the sound frequency ingredients of an audio on computer. The amplitude response of different frequencies can be freely modulated within specific range. Figure 1(c) shows that underwater communications relay on the frequency equalization process since the complex hydroacoustic environment needs frequency ingredients correction. Our proposed acoustic meta-equalizer is shown in Fig. 1(d). It consists of an acoustic metamaterial with several modulators. The latter are designed for specific amplitude control at different frequencies. By geometrically optimizing the metamaterial frame size and the parameters of HRs and FPRs, we can achieve high precise manipulations of the transmission coefficient for each octave. An integrated physical model is proposed to calculate the transmission for low and high frequencies, respectively. The corresponding analytical results agree well with the simulated and measured ones. Here, in analogy with conventional EQ device, we will show the realization of different functional filters, signal reproduction, and the modulation of specific sound effects by the AMEQ. Our finding integrating multiple functionalities will lead to real-world applications of acoustic metamaterials in room acoustics and architectural acoustics, *etc.*

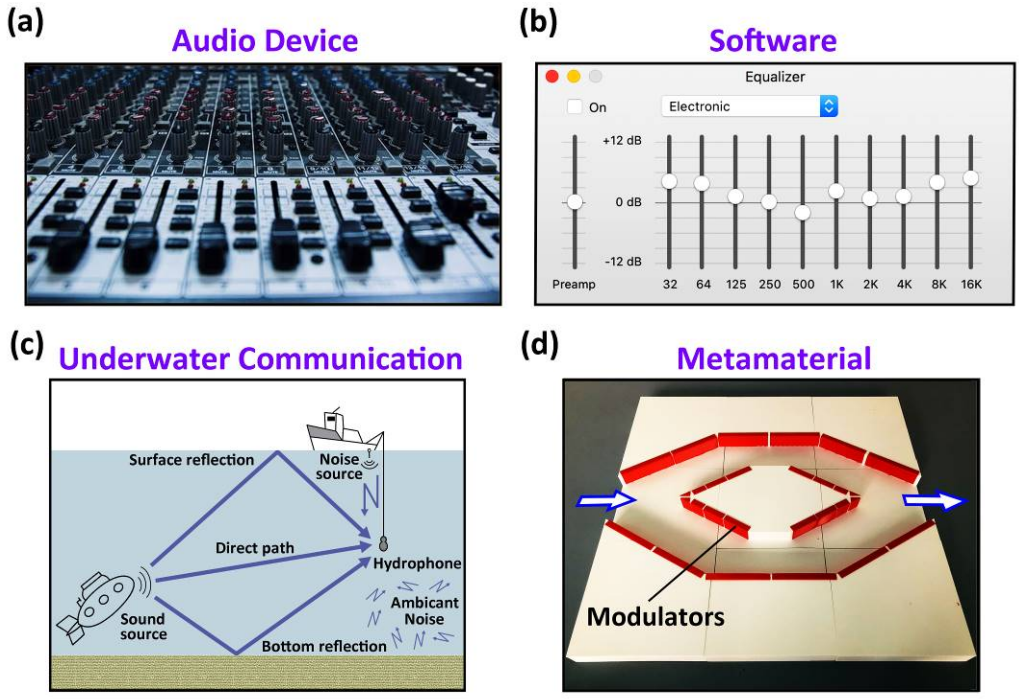

FIG. 1. The concept of equalizer. (EQ) with different potential applications. (a) EQ device in audio acoustics. (b) EQ software for sound effects control on computer. (c) Underwater acoustic communication relies on acoustic frequency equalization process. (d) Photography of the acoustic meta-equalizer (AMEQ), which is an acoustic metamaterial panel with several modulators.

II. RESULTS

A. Meta-structure design and analytical model

The conceived AMEQ is a two-port structure as schematically shown in Fig. 2(a). The acoustic wave is incident from one port and transmit to another port as the arrows indicate. The whole structure can be regarded as a "black box" with frequency equalization function. The two-dimensional (2D) structure is designed as a furcate channel with several modulators on both sides of the channel. The main difficulty and challenge for AMEQ design is that the modulators

should cover distinctly different resonant frequencies within ultra-broadband. Inspired by previous works, such as acoustic absorber and diffuser designs [20, 22], we introduce both HRs and FPRs as the low and high frequency modulators, respectively. Furthermore, in order to combine these two elements in an integrated structure, the furcate channel is deliberately designed with optimized geometry.

The modulators at the bottom and the top are used to control low frequencies (three center frequencies with f_1=250Hz, f_2=500Hz, and f_3=1000Hz). The modulators in the middle are exploited to modulate high frequencies (four center frequencies with f_4=2000Hz, f_5=4000Hz, f_6=8000Hz, and f_7=16000Hz). Figure 2(b) illustrates the three-dimensional (3D) structure of the AMEQ. The filters for different center frequencies (f_n) are marked in the figure. Figure 2(c) shows the air channel which is the complementary part of the solid structure in Fig. 2(b). Sound is propagating in the air channel. Figure 2(d) exhibits the whole 2D meta-structure of the AMEQ. Dashed box is the enlarged view of the solid box, showing the structural schematic diagram of each unit cell, with different geometrical parameters marked in the figure. The blue structure is corresponding to low frequencies. The corresponding filter structure is based on HRs with different sizes [29, 30]. The red structure is corresponding to high frequencies, and the corresponding filter structure is based on FPRs with different lengths [20, 31]. The whole structure is symmetrical in the four quadrants (marked by A, B, C, and D in Fig. 2(c)), so that each resonator has four same duplicates in the panel. Figure 2(e) shows the effective circuit model of the AMEQ, which is electrical element analogy [29, 30] corresponding to the analytical derivations we will present in the following section. The arrows indicate the input and output ports.

We achieve the precise modulation of the transmitted amplitude by optimizing the resonant

frequencies distributions f_{nm} of the different resonators as shown in Fig. 2(f), in which y-axis is scaled with log function. Red marks in Fig. 2(f) are the resonant frequencies f_{nm} of m^{th} HR unit cell of n^{th} (n=1,2,3) supercell contributing to n^{th} center frequency (f_n), while blue marks are the resonant frequencies f_{nm} of m^{th} FPR unit cell of n^{th} (n=4,5,6,7) supercell contributing to f_n. For example, for 6th center frequency (n=6, f=8000Hz), 6 resonators are designed with the resonant frequencies of f_{61}=6400Hz, f_{62}=7000Hz, f_{63}=7640Hz, f_{64}=8420Hz, f_{65}=9040Hz and f_{66}=9720Hz to ensure the broadband feature, as the blue marks in Fig. 2(f) display. The whole structure formed by these resonant frequency distributions can achieve precise modulations of amplitude with desired values.

To theoretically approach the properties of our concept, we investigate the specific resonators design with analytical expressions. For low frequency filters, a HR array is designed. As shown in Fig. 2(d), the three supercells of the HRs correspond to the three center frequencies (f_1-f_3), having 3, 4, and 10 HRs, respectively. In principle, the center frequency for each filter band is the average of resonant frequencies of different HRs, *viz.*, $f_n = \overline{f_{nm}}$, (n=1,2,3). The resonant frequency of HR is expressed as:

$$f_{nm} = \frac{1}{2\pi}\sqrt{\frac{1}{M_{nm}C_{nm}}}, \qquad (1)$$

where $M_{nm}=\rho_0 l_{nm}/w_{nm}$ and $C_{nm}=L_{nm}d_{nm}/\rho_0 c_0^2$ are acoustic masses and acoustic capacitances of the HR, respectively. ρ_0=1.21kg/m^3 and c_0=343m/s are the mass density and the sound speed of air, respectively. L_{nm} and d_{nm} are the height and the width of the cavity as marked in Fig. 2(d). l_{nm} and w_{nm} are the height and the width of the neck, respectively.

Then, the effective impedance of HRs in effective circuit model is calculated by [30, 32]:

$$Z_{nm}=i(\omega_{nm}M_{nm}-1/\omega_{nm}C_{nm})+R_{nm}, \qquad (2)$$

where $\omega_{nm}=2\pi f_{nm}$ are the angular frequencies, R_{nm} is the acoustic resistance induced by effects of

the radiation and thermal-viscosity. It can be formulated as:

$$R_{nm} \approx \frac{8L_{nm}}{\pi w_{nm}^{\ 2}}\sqrt{2\mu\omega_{nm}\rho_0} + 8\frac{\sqrt{2\mu\omega_{nm}\rho_0}}{\pi w_{nm}} + \frac{4\rho_0 c_0}{\pi w_{nm}}\left[1 - \frac{2J_1(k_{nm}w_{nm})}{k_{nm}w_{nm}}\right], \quad (3)$$

where μ=1.983×10^{-5}Pas is the dynamic viscosity of air, and J_1 is the Bessel function of the first kind. Combining the effective circuit model, we can explain the low frequency acoustic filter as the result of the sound reflection and the thermal-viscous loss (corresponding to the energy dissipation at $R_n = \bar{R}_{nm}$) at the resonances of the HRs (corresponding to the resonances of the circuit branch).

After obtaining the acoustic impedance Z_{nm} for each individual HRs, we can get the total effective impedance $Z(n)$ of the AMEQ for 3 different center frequencies.

$$Z(n) = \left(\sum_{j=1}^{m}\frac{1}{Z_{nm}}\right)^{-1}, \ (n = 1,2,3) \quad (4)$$

On the other hand, for the high frequency filters (red), an FPR array is designed. Similar to low frequency structure, the center frequency for each high frequency filter band is the average of all resonant frequencies of different FPRs $f_n = \bar{f}_{nm}$, (n=4,5,6,7). The length and the width is h_{nm} and w_{nm}, respectively. The filter frequency of FPR is expressed as [20]:

$$f_{nm} = \frac{c_0}{4h_{nm}} \quad (5)$$

The high frequency acoustic filter is directly decided by the sound abospotion in the FPR unit cells. On the other hand, the high frequency acoustic filter will be also influenced by multiple sound reflections in the integrated meta-structure. We characterize the high frequency acoustic filter by acoustic resistance $R_n = \bar{R}_{nm}$ (n=4, 5, 6, 7) in the effective circuit. The effective impedance of FPRs is calculated by [20]:

$$Z(n) = i\frac{\rho_0 c_0}{\omega}\left[\sum_m^M \frac{4\gamma\omega_{nm}}{(\omega_{nm}^2 - \omega^2 - i\beta\omega)(\pi M)}\right]^{-1}, \ (n = 4,5,6,7) \tag{6}$$

Here, γ is the ratio of the surface area occupied by FPR's cross sections to the effective surface area exposed to sounds. M *is* total number of the FPR for n^{th} center frenquency. β describes the weak system dissipation for the acoustic metamaterial.

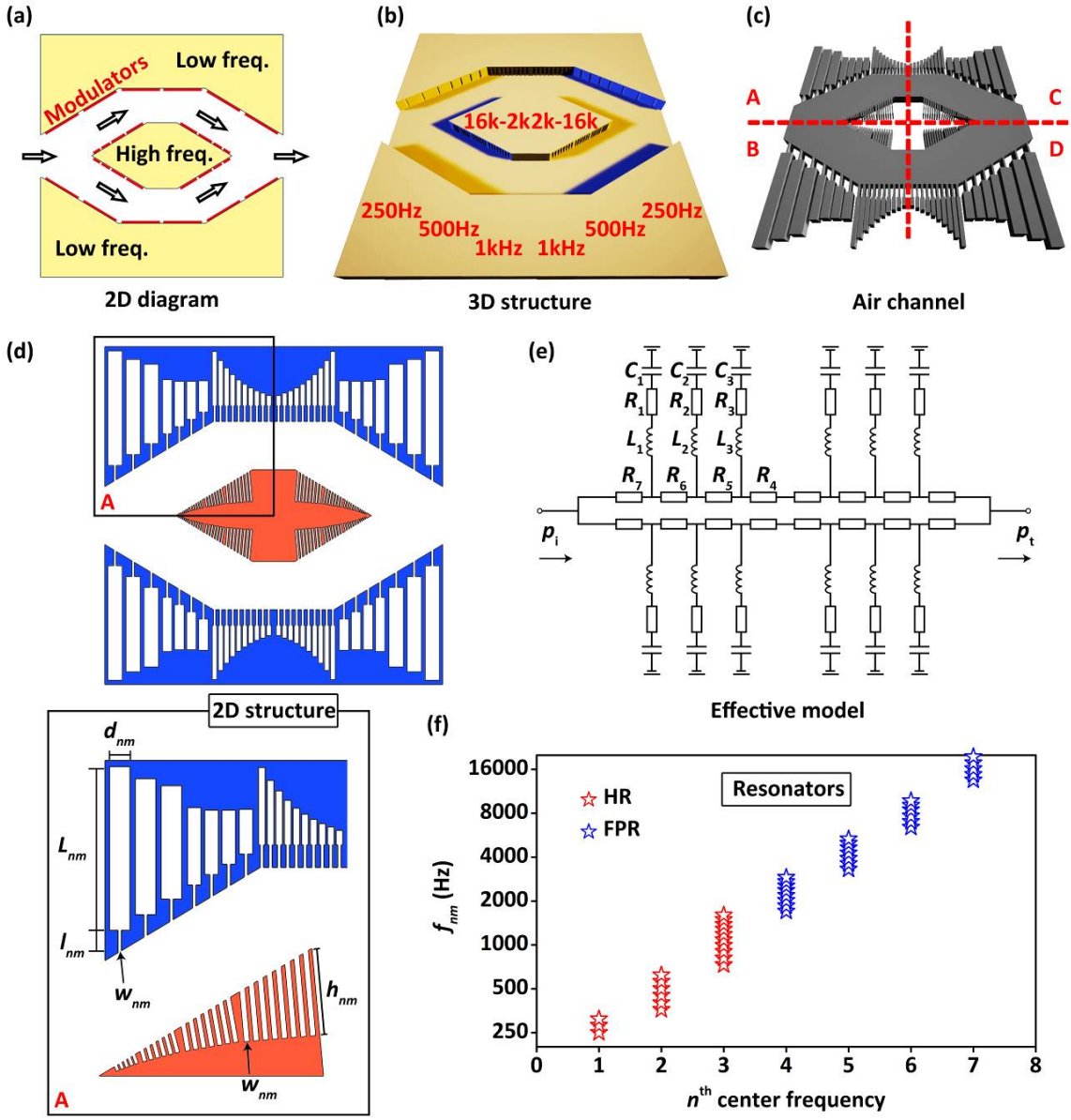

FIG. 2. The schematic diagram of the acoustic meta-equalizer (AMEQ). (a) The AMEQ device composed of a 2D channel structure with several modulators on the both sides of the waveguide. The modulators for high and low frequencies are marked. The arrows indicate the transmission directions. (b) The 3D structure of the AMEQ. The filters for the different center frequencies are marked. (c) The 3D structure of the air channel in which the sound is transmitted. The whole structure is symmetrical in the four quadrants marked by A, B, C, and D. (d) 2D structure of AMEQ. Dashed box is the enlarged view of the solid box, showing the structural schematic diagram of the unit cell, with different geometrical parameters marked in the figure. (e) The effective circuit model of the AMEQ. The arrows indicate the input and output ports. (f) The optimized resonant frequencies distributions f_{nm} of HRs (red marks) and FPRs (blue marks), for n^{th} center frequencies. *Y*-axis is scaled with log function.

We, then, can modulate the transmission coefficient (acoustic presure amplitude) by controlling the turn on and turn off states of each resonantor using the modulators. Since each resonator has four same duplicates in A, B, C, D quadrants in the panel. The number of the activated (turned on) resonantors can be chosen as $\delta(n)$=0, 1, 2, 3, or 4. Thus, based on the effective acoustic impedance $Z(n)$, the transmission $T(n)$ of the AMEQ for n^{th} center frequencies are related to the number of $\delta(n)$, calculated as:

$$T(n) = T_0, (\delta(n) = 0) \tag{7a}$$

$$T(n) = T_0 \left[\frac{Z(n)}{Z(n)+\rho_0 c_0} \right], (\delta(n) = 1) \tag{7b}$$

$$T(n) = T_0 \left[\frac{Z(n)-\rho_0 c_0}{Z(n)+\rho_0 c_0} \right], (\delta(n) = 2) \tag{7c}$$

$$T(n)=T_0\left[\frac{Z(n)(Z(n)-\rho_0c_0)}{(Z(n)+\rho_0c_0)^2}\right],(\delta(n)=3) \quad (7d)$$

$$T(n)=T_0\left[\frac{Z(n)-\rho_0c_0}{Z(n)+\rho_0c_0}\right]^2,(\delta(n)=4) \quad (7e)$$

Here, T_0 is the transmission of a pure channel without any resonators as shown in Fig. 3(a). Because the channel has an unusual shape, the transmission curve of T_0 is not planar, but related to the working frequency, as shown in Fig. 3(b), with the averaged closed to 0.8. Here, we assume T_0=0.8 to simplify the following analytical calculations. From the curve of T_0, one can see the transmission above 1890Hz is oscillating because it is the approximate cutoff frequency of the channel. Therefore, the low frequency filters from 180Hz to 1890Hz are owing to the resonance of the whole structure. The high frequency filters from 1890Hz to 22000Hz are determined by both the resonance of FPR element as well as geometrical acoustics effects. This is reflected in the parameter γ in Eq. (6), that is, an effective filling rate related to the geometric feature of the channel and the distribution of FPRs. In this case, the filling rate γ is smaller than the previous case for a compact structure [20].

B. Amplitude Control

Owing to the precise modulations by the optimized resonator arrays, the transmitted amplitude is controlled with Levels 0-4 corresponding to amplitudes A=0.8, 0.63, 0.5, 0.4, 0.3 (*viz.*, -2dB, -4dB, -6dB, -8dB, -10dB, respectively). Figure 3(c) shows the schematic diagram for Levels 0-4. In this diagram, the 28 circles represent 28 modulators for different f_n (each frequency has 4 tunable modulators). The red circles represent turn off states, for which we fix a red slice covering the opening of the resonator to prevent the effect of the resonator. The gray

circles represent turn on states, indicating no slice is fixed. The photographs of the samples for Levels 0-4 are also shown in Fig. 3(c). The sample is tunable by introducing the red slices as modulators [33]. It has a size of 56cm×56cm×4cm (Horizontal size 56cm is about 1/4 wavelength of the lowest working frequency). The samples and the slices are made by 3D printer with polylactic acid (PLA) having the mass density ρ=1250kg/m^3, Young's modulus E=3.2×10^{9}Pa, and Poisson's ratio v=0.35.

The simulations were performed using commercial finite element analysis software COMSOL Multiphysics 5.4a with the "Acoustic-Thermoviscous Acoustic Interaction, Frequency Domain" and "Thermoviscous Acoustic-Solid Interaction, Frequency Domain" modules. The considered mass density and the sound speed of background medium air are ρ_0=1.21kg/m^3 and c_0=343m/s, respectively.

The simulated, analytical, and measured filter curves for 5 samples are shown in Fig. 3(c). The transmission for one center frequency, such as 8000Hz, is obtained by calculating the averaged acoustic pressure amplitude within one octave from 5657Hz to 11314Hz (with a step of 1/24 octave, *viz.*, 25 frequencies). For the experiment, the measurements are carried out in 2D parallel waveguide experimental system [33]. The distance between two parallel waveguides is 4cm. The size of the parallel waveguides is 0.6m×0.8m. Sound-absorbing cotton is placed at the boundaries of the parallel waveguides to prevent undesired reflections. A 10cm-diameter loudspeaker (matches with the input side size 9.6cm) is fixed at the input boundary of the sample. The acoustic wave is generated continuously and the static acoustic field is measured.

The output cross-section of the sample is scanned to obtain the output average acoustic wave amplitude, with 1/4-inch-diameter Brüel&Kjær type-4961 microphone and Brüel&Kjær PULSE Type 3160. Brüel&Kjær software is used for measurement, in which "Constant

Percentage Bandwidth Analyzer" (CPB) is chosen that the incident frequency is sweeping from 180Hz to 22000Hz. One can conveniently measure the averaged acoustic pressure amplitude in real-time for every octave from f_1=250Hz to f_7=16000Hz. The results in Fig. 3(c) show that, by controlling the number of the modulators (0, 7, 14, 21, and 28, respectively), we can achieve predesigned amplitude response (0.3-0.8) at the output side.

The analytical results agree with the simulated and experimental ones. It is noted that the simulated amplitudes for 1000Hz and 2000Hz are slightly higher than the predesigned ones. This is an inevitable error, due to the fact that Level 0 is corresponding to the pure channel case, whose transmission T_0 is not exactly planar as shown in Fig. 3(b), but with higher values around 1000Hz-2000Hz. One solution to further improve the amplitude curve is to use modified profiles of the activated modulators as shown in Fig. 3(e). The amplitude controls based on modified profiles are more precise. Anyhow, the results in Fig. 3(d) are already sufficient to show the ability of the proposed structure to control the sound transmission with specific values with small error for each targeted center frequency, respectively. The realization of the amplitude control is the foundation for other more complex acoustic equalization operations.

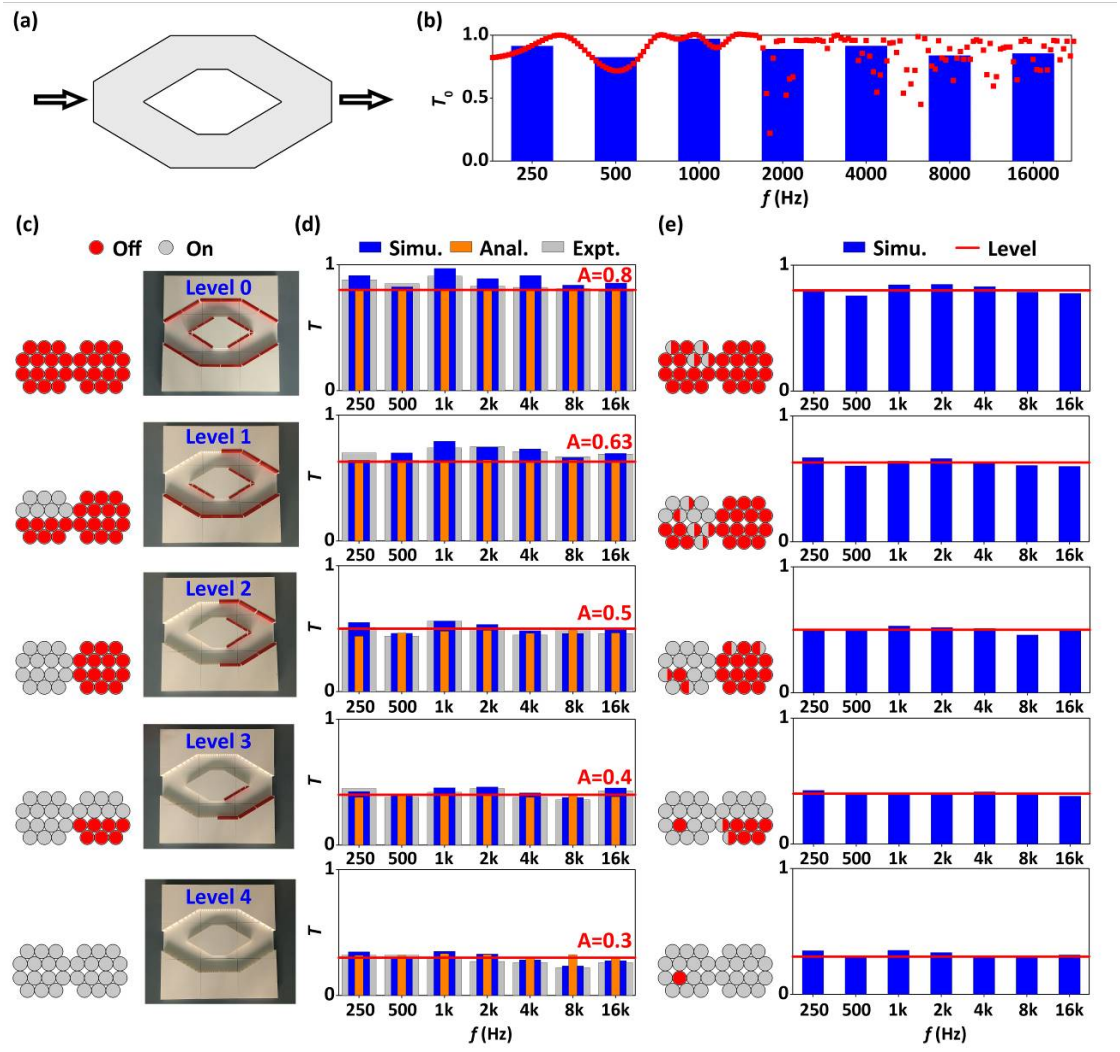

FIG. 3. Amplitude Control. (a) The pure channel without any resonators. (b) The transmission of the pure channel without any resonators. *X*-axis is scaled with log function. (c) The schematic diagram of modulators distribution and the photographs of the samples. (d) The simulated, analytical, and experimental results of the amplitude response at different octaves. The amplitude responses are modulated as Levels 0-4 with A=0.8, 0.63, 0.5, 0.4, and 0.3, respectively. (-2dB, -4dB, -6dB, -8dB, and -10dB respectively). The predesigned EQ values are displayed by red solid lines. (e) The simulated results of the amplitude response at different octaves for the modified profiles.

C. Functional filter

Different functional filters are important elements in signal processing [1], such as the classical ones, *i.e.*, high-pass, low-pass, band-pass, and stop-band. In the following, we show the realizations of the above four functional filters. The schematic diagram and the samples are shown in Fig. 4(a) and 4(d). The distributions of the modulators are optimized to achieve the desired filter curve. The high-pass filter is designed as high-transmission for 4 octaves with center frequencies from 2000Hz to 16000Hz, while low-transmission is designed for 3 octaves with center frequencies from 250Hz to 1000Hz. In Fig. 4(e), the numerical and experimental results show that the amplitude response for 200Hz-1400Hz is about A=0.3, and for 1400Hz-20000Hz is about A=0.6. Similar designs are applied to other filters in Fig. 4(f). The low-pass filter has A=0.8 for 200Hz-1400Hz, and A=0.45 for 1400Hz-20000Hz. Regarding the band-pass filter, it produces a high-transmission band within two octaves (1000Hz and 2000Hz), and low-transmission for the other octaves. In Fig. 4(g), the numerical, analytical, and experimental results show that the amplitude responses are approximately A=0.75 for 700Hz-2800Hz, and A=0.45 for the other bandwidths (200Hz-700Hz and 2800Hz-20000Hz). On the contrary, stop-band filter in Fig. 4(h) has a low-transmission band within two octaves (1000Hz and 2000Hz), and produces high-transmission for the other octaves. The numerical and experimental results show that the amplitude responses are approximately A=0.35 for 700Hz-2800Hz, and A=0.65 for other bandwidths (200Hz-700Hz and 2800Hz-20000Hz). The realization of such functional filters will lead to applications in noise control with tunable frequency ranges.

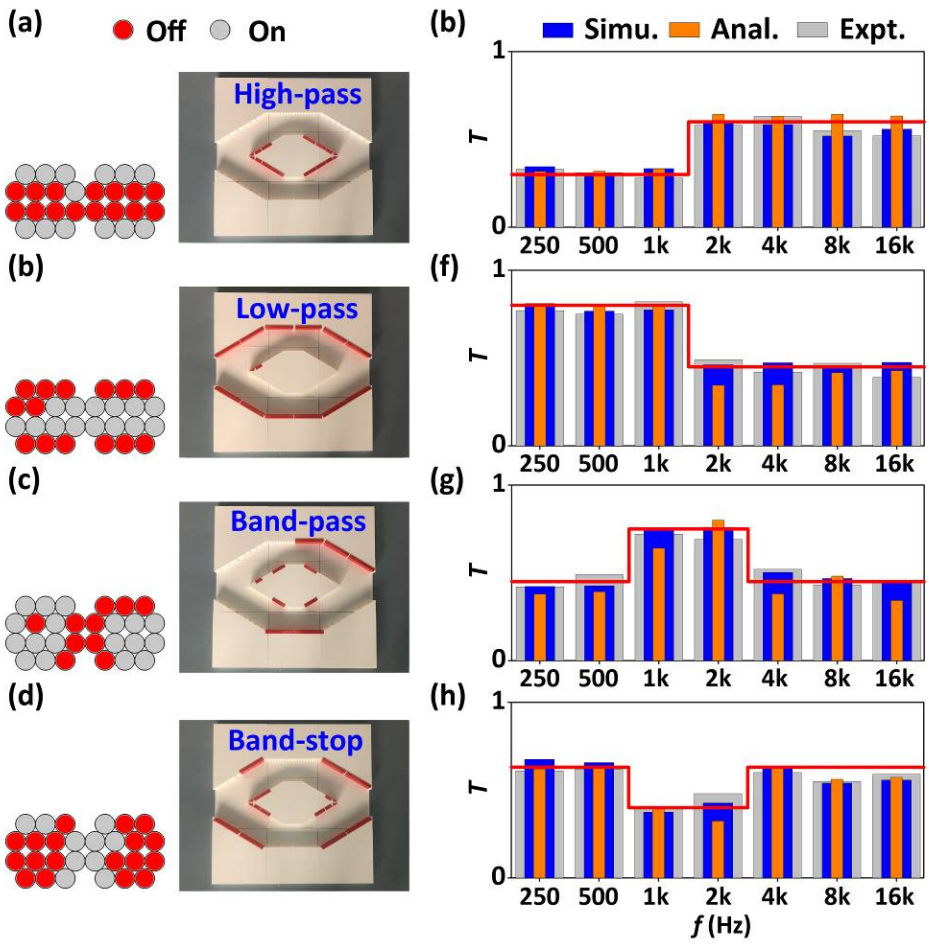

FIG. 4. Functional filter. (a-d) The schematic diagram of modulators distribution and the photographs of the samples. (e-h) The simulated, analytical, and experimental results of the samples for different functional filters, *viz.*, high-pass, low-pass, band-pass, and band-stop, respectively. The predesigned EQ values are displayed by red solid lines.

D. Signal reproduction

Signal reproduction is an important concept proposed in room acoustics [8], that uses an equalization process to reproduce the input signal with random or unbalanced frequency ingredients, and reconstructs it as a balanced one with a planar frequency response curve. Figure 5(a) shows two examples of predesigned original incident signals (oscillating shapes) with

unbalanced frequency ingredients, while Fig. 5(b) illustrates two optimized samples to reproduce the input signal. The frequency response features of the samples need to be complementary to the input signals. Regarding the results, Fig. 5(c) summarizes simulated, analytical, and experimental EQ curves of the designed samples, which agree with the predicted complementary curves. These results are obtained by comparing the output signal with a balanced input signal on the samples. Figure 5(b) shows the simulated and experimental results for sound reproduction, which are obtained by comparing the output signal with the unbalanced input signals of Fig. 5(a). The numerical and experimental results evidence that the reproduced signal has a planar frequency response, showing the effectiveness of the optimized structures represented in Fig. 5(b) for signal reproduction.

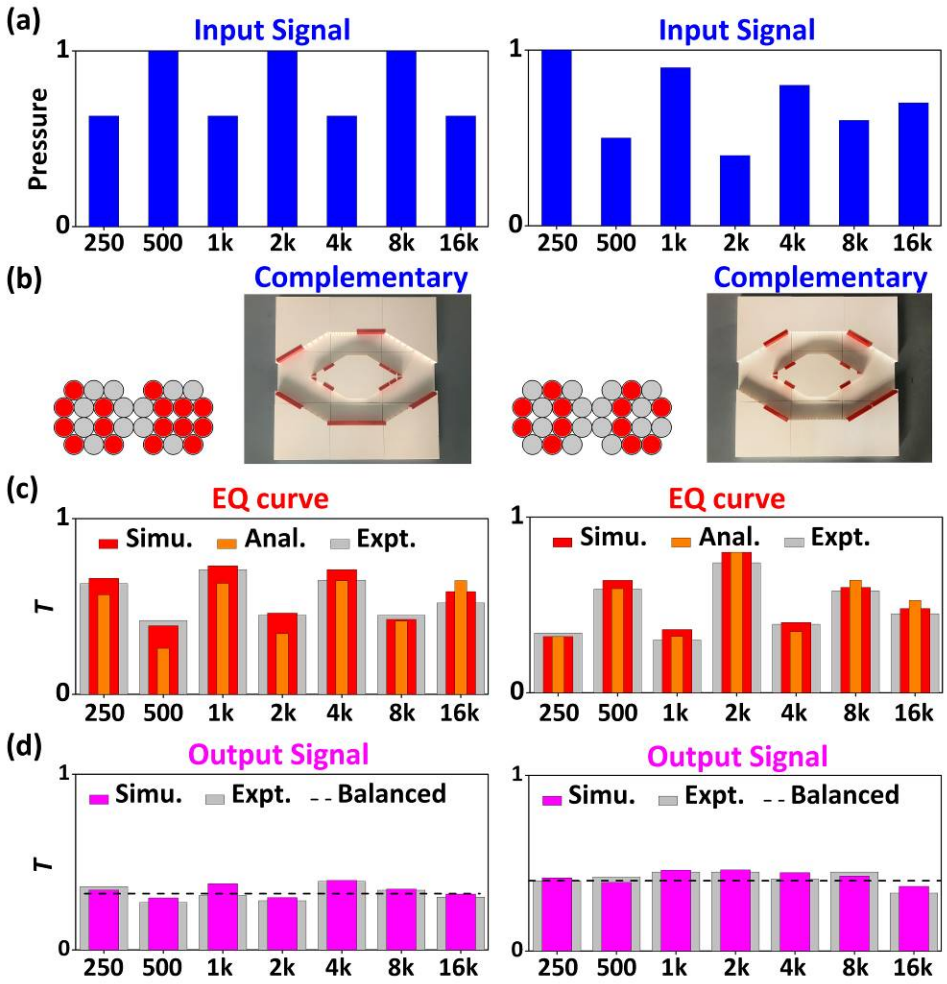

FIG. 5. Signal reproduction. (a) The input signals with unbalanced frequency amplitude ingredients. (b) The schematic diagram of modulators distribution and the photographs of the complementary samples. (c) The simulated, analytical, and experimental results of the EQ curve of samples for the signal reproduction. (d) The simulated and experimental transmissions of output signals after the signal reproduction. The predesigned output values are displayed by black dashed lines.

E. Sound effect control

Sound effect control [5] is another fascinating application of EQ device which requires a fine modulation of each frequency ingredient. We predesign four EQ curves (denoted as

EQ1-EQ4) whose sound effects are famous in music productions, *viz.*, EQ1 (Hip-hop), EQ2 (Popular), EQ3 (R&B), and EQ4 (Dance), respectively. The AMEQ structures as well as the simulated, analytical, and measured data are illustrated in Figs. 6(a-h). By the optimizing the modulators distribution, we obtain the desired EQ curves at the output side of the AMEQ. The results show that the low frequency control is more precise than the high-frequency one (such as the results at 16kHz). This is due to the fact that high frequency filter is more sensitive to the plane wave incident waveform (direction). The ability of the real sound effect control by AMEQ is significant for the applications in architectural acoustics, when the high-quality hearing effect is desired.

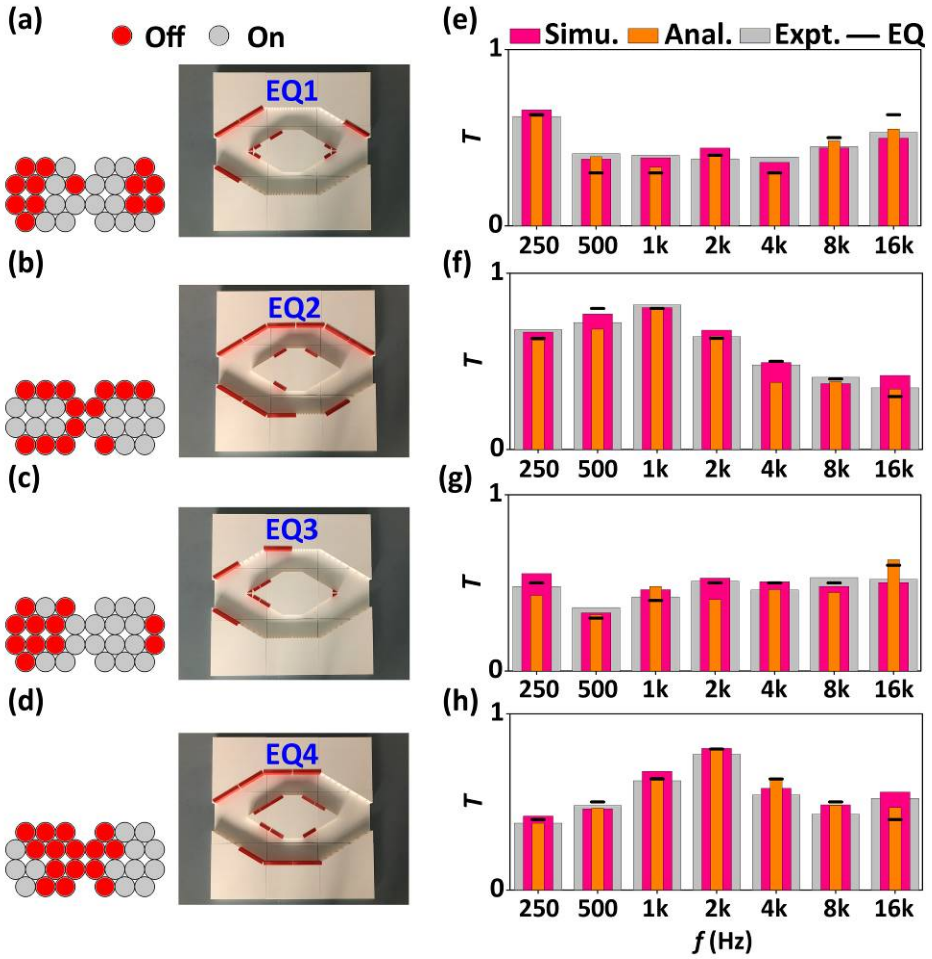

FIG. 6. Sound effect control. (a-d) The schematic diagram of modulators distribution and the

photographs of the samples. (e-h) The simulated, analytical, and experimental results of the EQ curve of the samples for different sound effects, *viz.*, EQ1 (Hip-hop), EQ2 (Popular), EQ3 (R&B), and EQ4 (Dance), respectively. The predesigned EQ values are displayed by black solid line.

III. DISCUSSION AND CONCLUSION

We have proposed the unique concept of acoustic meta-equalizer capable of providing acoustic wave equalization with a passive acoustic metamaterial. The equalization requires tunable and ultra-broadband frequency filter. By using two kinds of acoustic resonant unit cells (Helmholtz resonators and Fabry–Perot resonators), we have realized ultra-broadband filters within a fully integrated structure. The optimization of the resonators design ensures highly precise amplitude modulations. The obtained bandwidth can reach 7 octaves, *viz.*, 200Hz-20000Hz, while the amplitude can be modulated with 5 levels (-2dB to -10dB with the step of -2dB) realized by tuning 28 modulators. It's worth mentioning that the tunability of the current system is manual via designed slices. For further improving the tunability of the system, a possible method is to introduce origami structure [34] to switch the "turn on" and "turn off" states of the system by using folding slices. The bandwidth and the degree of freedom of amplitude outperform conventional acoustic filters. In analogy with the equalization applications in communication systems, room acoustics, and audio device, we have numerically and experimentally demonstrated and provided the proof-of-concept of functional filters, signal reproduction, and sound effect control, respectively. The proposed concept of acoustic meta-equalizer aims to connect acoustic metamaterials to the practical acoustic applications. Although the precision of the proposed meta-equalizer is not as high as the matured electronic

counterpart, the proposed meta-equalizer may have unique applications in architectural acoustics. For example, a passive structure with ultra-broadband feature is a good candidate for noise control with controllable frequency spectrum. The concept of equalizer extended from electronic device to acoustic meta-device will lead to more possible applications, such as noise control with ventilation property [35-36], beyond the applications of conventional electronic equalizer.

ACKNOWLEDGMENTS

This work is supported by the Air Force Office of Scientific Research under award number FA9550-18-1-7021, and by la Région Grand Est and Institut Carnot ICEEL.

References

1. S. U. H. Qureshi, Adaptive equalization. Proc. of the IEEE **73**, 1349-1387 (1985).
2. D. Falconer, S. L. Ariyavisitakul, A. Benyamin-Seeyar, B. Eidson, Frequency domain equalization for single-carrier broadband wireless systems. IEEE Commun. Mag. **40**, 58-66 (2002).
3. https://en.wikipedia.org/wiki/Equalization
4. F. Everest, The master handbook of acoustics (Blue Ridge Summit: TAB Books, 1981).
5. D. Howard and J. Angus, Acoustics and Psychoacoustics (Focal, London, 1999).
6. B. D. Radlovic, R. C. Williamson, R. A. Kennedy, Equalization in an acoustic reverberant environment: Robustness results. IEEE Trans. Speech Audio Process. **8**, 311-319 (2000).
7. F. Talantzis, D. B. Wardm, Robustness of multichannel equalization in an acoustic reverberant environment. J. Ac. Soc. Am. **114**, 833-841 (2003).
8. S. Spors, H. Buchner, R. Rabenstein, W. Herbordt, Active listening room compensation for massive multichannel sound reproduction systems using wave-domain adaptive filtering. J. Ac. Soc. Am. **122**, 354-369 (2007).
9. S. M. Kuo, D. R. Morgan, Active noise control systems. (Wiley, New York, 1996).
10. M. Bouchard, Multichannel affine and fast affine projection algorithms for active noise control and acoustic equalization systems. IEEE Trans. Speech Audio Process. **11**, 54-60 (2003).

11. M. Stojanovic, J. Catipovic, J. G. Proakis, Adaptive multichannel combining and equalization for underwater acoustic communications. J. Ac. Soc. Am. **94**, 1621-1631 (1993).

12. M. Chitre, S. Shahabudeen, M. Stojanovic, Underwater acoustic communications and networking: Recent advances and future challenges. Mar. Technol. Soc. J. **42**, 103-116 (2008).

13. G. C. Ma and P. Sheng, Acoustic metamaterials: From local resonances to broad horizons. Sci. Adv. **2**, e1501595 (2016).

14. S. A. Cummer, J. Christensen, A. Alù, Controlling sound with acoustic metamaterials. Nat. Rev. Mat. **1**, 16001 (2016).

15. Y. B. Xie, T. Tsai, A. Konneker, B. Popa, D. Brady, S. A. Cummer, Single-sensor multispeaker listening with acoustic metamaterials. Proc. Natl. Acad. Sci. USA **112**, 10595–10598 (2015).

16. G. C. Ma, X. Y. Fan, P. Sheng, M. Fink, Shaping reverberating sound fields with an actively tunable metasurface. Proc. Natl. Acad. Sci. USA **115**, 6638–6643 (2018).

17. Y. F. Zhu, J. Hu, X. D. Fan, J. Yang, B. Liang, X. F. Zhu, J. C. Cheng, Fine manipulation of sound via lossy metamaterials with independent and arbitrary reflection amplitude and phase. Nat. Commun. **9**, 1632 (2018).

18. C. Z. Shi, M. Dubois, Y. Wang, X. Zhang, High-speed acoustic communication by multiplexing orbital angular momentum. Proc. Natl. Acad. Sci. USA **114**, 7250 (2017).

19. X. Jiang, B. Liang, J. C. Cheng, C. W. Qiu, Twisted acoustics: metasurface-enabled multiplexing and demultiplexing. Adv. Mater. **30**, 1800257 (2018).

20. M. Yang, S. Y. Chen, C. X. Fu, P. Sheng, Optimal sound-absorbing structures. Mater. Horizons **4**, 673 (2017).

21. B. Assouar, B. Liang, Y. Wu, Y. Li, J. C. Cheng, Y. Jing, Acoustic metasurfaces. Nat. Rev. Mat. **1**, 460–472 (2018).

22. Y. F. Zhu, X. D. Fan, B. Liang, J. C. Cheng, Y. Jing, Ultrathin acoustic metasurface-based Schroeder diffuser. Phys. Rev. X **7**, 021034 (2017).

23. T. Cox, P. D'Antonio, Acoustic absorbers and diffusers: theory, design and application. (Crc Press, New York, 2016).

24. Y. Li and B. Assouar, Acoustic metasurface-based perfect absorber with deep subwavelength thickness. Appl. Phys. Lett. **108**, 063502 (2016).

25. G. C. Ma, M. Yang, Z. Y. Yang, P. Sheng, Low-frequency narrow-band acoustic filter with large orifice. Appl. Phys. Lett. **103**, 011903 (2013).

26. Z. Q. Liu, H. Zhang, S. Y. Zhang, L. Fan, An acoustic dual filter in the audio frequencies with two local resonant systems. Appl. Phys. Lett. **105**, 053501 (2014).

27. B. Assouar, M. Senesi, M. Oudich, M. Ruzzene, Z. L. Hou, Broadband plate-type acoustic metamaterial for low-frequency sound attenuation. Appl. Phys. Lett. **101**, 173505 (2012).

28. G. Y. Song, Q. Cheng, B. Huang, H. Y. Dong, T. J. Cui, Broadband fractal acoustic metamaterials for low-frequency sound attenuation. Appl. Phys. Lett. **109**, 131901 (2016).

29. Y. F. Zhu and B. Assouar, Multifunctional acoustic metasurface based on an array of Helmholtz resonators. Phys. Rev. B **99**, 174109 (2019).

30. Y. F. Zhu and B. Assouar, Systematic design of multiplexed-acoustic-metasurface hologram with simultaneous amplitude and phase modulations. Phys. Rev. Mater. **3**, 045201 (2019).

31. X. Jiang, B. Liang, R. Q. Li, X. Y. Zou, L. L. Yin, J. C. Cheng, Ultra-broadband absorption by acoustic metamaterials. Appl. Phys. Lett. **105**, 243505 (2014).

32. L. Kinsler, Fundamentals of Acoustics (Wiley, New York, 1982).

33. S. W. Fan, S. D. Zhao, A. L. Chen, Y. F. Wang, B. Assouar, Y. S. Wang, Tunable broadband reflective acoustic metasurface. Phys. Rev. Appl. **11**, 044038 (2019).

34. Y. F. Zhu, F. Fei, S. W. Fan, L. Y. Cao, K. Donda, and B. Assouar, Reconfigurable origami-inspired metamaterials for controllable sound manipulation. Phys. Rev. Appl. **12**, 034029 (2019).

35. T. Lee, T. Nomura, E. M. Dede, and H. Iizuka, Ultrasparse acoustic absorbers enabling fluid flow and visible-light controls. Phys. Rev. Appl. **11**, 024022 (2019).

36. M. Sun, X. S. Fang, D. X. Mao, X. Wang, and Y. Li, Broadband acoustic ventilation barriers. Phys. Rev. Appl. **13**, 044028 (2020).